


CrossMark  
click for updates

Cite this: DOI: 10.1039/c4sm01693a

# How does growth hormone releasing hexapeptide self-assemble in nanotubes?

Héctor Santana,<sup>a</sup> Cesar L. Avila,<sup>b</sup> Ingrid Cabrera,<sup>cd</sup> Rolando Páez,<sup>a</sup> Viviana Falcón,<sup>a</sup> Adalberto Pessoa Jr.,<sup>e</sup> Nora Ventosa,<sup>cd</sup> Jaume Veciana,<sup>cd</sup> Rosangela Itri<sup>f</sup> and Leandro Ramos Souza Barbosa<sup>\*f</sup>

Growth hormone releasing peptide, GHRP-6, a hexapeptide (His-(D-Trp)-Ala-Trp-(D-Phe)-Lys-NH<sub>2</sub>, MW = 872.44 Da) that belongs to a class of synthetic growth hormone secretagogues, can stimulate growth hormone secretion from somatotrophs in several species including humans. In the present study, we demonstrate that GHRP-6 dispersed in aqueous solution, at pH 7.0, room temperature of 22 °C, is able to form long nanotubes, which is evidenced by combining small angle X-ray scattering (SAXS), transmission electron microscopy and molecular dynamics simulation results. Such nanotubes possess inner and outer cross-sections equal to 6.7(2) nm and 13.4(5) nm, respectively. The mechanism of peptide self-assembly was determined by molecular dynamics simulations revealing that the peptides self-assemble like amphiphilic molecules in aqueous solution in a partially interdigitated structure. In this case, the position of the positively charged amino terminus is located at the peptide–water interface, whereas the neutral NH<sub>2</sub>-capped carboxy terminus remains buried at the hydrophobic core. In contrast, the long side chain of Lys-6 stretches out of the hydrophobic core positioning its positive charge near the cylinder surface. The peptide configuration in the nanotube wall comes from the interplay between the hydrophobic interactions of the aromatic side chains of GHRP-6 and the electrostatic repulsion of its cationic charges. On increasing the peptide concentration, the long nanotubes self-arrange in solution displaying a bi-dimensional hexagonal-like packing in the SAXS curves, with a center-to-center distance of ~15 nm. Further, we also show that the nanostructure formed in solution is quite stable and is preserved following transfer to a solid support.

Received 30th July 2014  
Accepted 16th September 2014

DOI: 10.1039/c4sm01693a

www.rsc.org/softmatter

## 1. Introduction

Molecular self-assembly is one of the most powerful approaches nowadays to construct advanced functional biomaterials of nanoscale dimension.<sup>1–3</sup> Among several different molecules, peptides are outlined as excellent building-blocks for nanotechnology applications, due to their well-known synthesis, small size, chemical flexibility and versatility, biocompatibility, biological recognition abilities and relatively easy chemical and biological modifiability.<sup>4,5</sup> For instance, the structural

properties of self-assembled peptides have been exploited due to the formation of quite different structures such as nanotubes,<sup>6,7</sup> nanospheres, nanofibers,<sup>8</sup> scaffolds,<sup>9,10</sup> nanoribbons,<sup>11</sup> nanotapes,<sup>12</sup> hydrogels,<sup>13,14</sup> or even self-assembled vesicle-capped nanotubes that can be selectively disassembled by irradiation as reported by Coleman *et al.*<sup>15</sup>

Besides their nanotechnological relevance, self-assembled peptides have also been implicated in health sciences for therapeutic and diagnostic applications,<sup>16</sup> as well as for cosmetic applications.<sup>17</sup> Some peptides also have the ability to form fibers and gels, composed of elongated structures (like micelles), which could be used for tissue engineering and regenerative medicine applications.<sup>16,18</sup>

In this scenario, Growth Hormone Releasing Hexapeptide, GHRP-6 (Fig. 1), belongs to a class of synthetic growth hormone secretagogues (GHSs), which stimulate growth hormone (GH) release from somatotrophs in a dose-dependent manner in several species including humans.<sup>19</sup> There are some indications of a potential therapeutic option of GHRP-6 in the prevention and treatment of heart failure,<sup>20,21</sup> an effect that seems to be related to an enhanced non-ischemic compensatory mechanism and mediated *via* specific GH secretagogue receptors

<sup>a</sup>Department of Pharmaceutical Technology, Center for Genetic Engineering and Biotechnology, Ave 31/158 and 190, PO Box. 6162, Havana 10600, Cuba

<sup>b</sup>Instituto Superior de Investigaciones Biológicas (INSIBIO), CCT-Tucumán and Instituto de Química Biológica Dr Bernabé Bloj (CONICET-UNT), Chacabuco 461, T4000ILI Tucumán, Argentina

<sup>c</sup>Department of Molecular Nanoscience and Organic Materials (ICMAB-CSIC), Bellaterra, 08193, Spain

<sup>d</sup>CIBER de Bioingeniería, Biomateriales y Nanomedicina (CIBER-BBN), Bellaterra, 08193, Spain

<sup>e</sup>Department of Biochemical and Pharmaceutical Sciences, School of Pharmaceutical Sciences, University of São Paulo, Brazil

<sup>f</sup>Instituto de Física, Universidade de São Paulo, Cx. Postal 66318, CEP 05315-970, São Paulo, Brazil. E-mail: lbarbosa@if.usp.br; Tel: +55 11 30917157

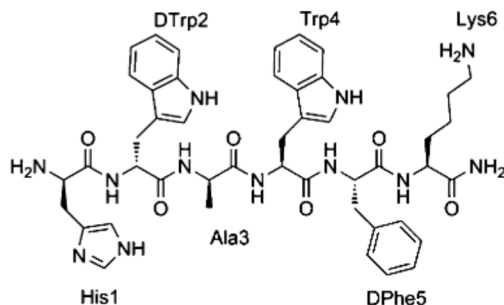


Fig. 1 Schematic representation of GHRP-6.

rather than *via* the GH/IGF-1 pathway. Besides, a recent study indicates that the combined administration of the GHRP-6 peptide and EGF (epidermal growth factor), which can protect cells from apoptosis,<sup>22</sup> resulted in an effective alternative for recovery from amyotrophic lateral sclerosis (ALS),<sup>23</sup> although further preclinical investigation must be carried out.<sup>23</sup> Of note, ALS is a central nervous system (CNS) disease characterized by irreversible loss of spinal motor neurons with an evolution of the patient to death in a few years,<sup>24,25</sup> with no effective treatment reported until now.

In spite of the relevance of GHRP-6, there is a lack in the literature concerning its probable self-organization in the physiological environment. In this context, in the current study we focus our attention on the properties of GHRP-6 self-assembly in aqueous solution combining experimental and molecular dynamics (MD) simulation data. The self-aggregation features of GHRP-6 dispersed in phosphate buffer solution, at pH 7.4, were investigated by the small angle X-ray scattering (SAXS) technique combined with cryogenic and conventional Transmission Electron Microscopy (Cryo-TEM and TEM) performed on dried samples. SAXS is a low-resolution technique that allows us to access both the shape and dimension of the scattering object, whereas Cryo-TEM and TEM can reveal small morphological changes as, for instance, twisted-to-helical transition as reported elsewhere.<sup>26</sup> The results revealed that GHRP-6 peptides form elongated linear structures with inner and outer cross-sections of 7 (1) and 13 (1) nm, respectively. Such dimensions were used as constraints to infer the self-assembly mechanism at the molecular level by MD. Interestingly, MD evidenced a partially interdigitated peptide in a nanotube-like configuration, resulting from the interplay between the hydrophobic interactions of the aromatic side chains of GHRP-6 and the electrostatic repulsion of the cationic charges (Fig. 1). Knowledge of the peptide self-assembly mechanism can pave the way for future bio-inspired materials with potential technological applications.

## 2. Materials and methods

### 2.1 Sample preparation

GHRP-6 was obtained from BCN Peptides (Barcelona, Spain) as the acetate salt and used as received. The GHRP-6 solutions were prepared by dissolving the desired amount of peptide in 20

mM phosphate buffer at pH 7.4. GHRP-6 concentration was determined from UV-Vis spectrometric measurements at 280 nm, using the molar extinction coefficient obtained from the amino acid composition ( $\epsilon_{280} = 11\,120\text{ M}^{-1}\text{ cm}^{-1}$ ). For TEM and Cryo-TEM analyses the samples were incubated at room temperature of 22 °C for about one day prior to the measurements. All reagents were of analytical grade and used without further purification.

### 2.2 Transmission electron microscopy

TEM negative staining was performed as follows: an initial layer on a copper grid was coated with carbon. The grid was immersed in 20  $\mu\text{L}$  of the sample and blotted after 1 min. The grid was washed with water for 1 min and then blotted to remove excess of the protein material. To enhance the contrast, the grid was immersed in 2% (w/w) uranyl acetate and blotted after 1 min. Examination was performed using a JEOL JEM-2000 EX transmission electron microscope (Jeol Ltd, Tokyo, Japan) operating at 80 kV.

Cryo-TEM images were obtained using a JEOL JEM-2011 transmission electron microscope (Jeol Ltd, Tokyo, Japan) operating at 120 kV. A small drop of the sample was placed on a copper grid coated with a perforated polymer film. Excess solution was thereafter removed by blotting with filter paper. Immediately after film preparation, the grid was plunged into liquid ethane held at a temperature just above its freezing point (94 K). The vitrified sample was then transferred to the microscope for analysis. To prevent sample perturbation and the formation of ice crystals, the specimens were kept cold (77 K) during both the transfer and viewing procedures. Samples composed of 20  $\text{mg mL}^{-1}$  of GHRP-6 peptides in phosphate buffer solution, pH 7.4, were submitted to TEM and Cryo-TEM measurements after incubation for about one day at temperatures from 2 to 8 °C.

TEM and Cryo-TEM images were analyzed using Gatan Digital Micrograph 1.8 software. The tools of this software allowed us to measure both inner and outer cross-sections of each aggregate independently. Accordingly, histograms and corresponding Gaussian fits were obtained by using OriginPro 8.0. A total of 85 and 40 linear aggregates were analyzed through Cryo-TEM and TEM images, respectively.

### 2.3 Small-angle X-ray scattering

Small Angle X-ray Scattering (SAXS) data from phosphate buffer solutions containing GHRP-6 at 20, 30, 50 and 70  $\text{mg mL}^{-1}$ , pH 7.4, were obtained on the SAXS2 beamline at the Laboratório Nacional de Luz Síncrotron (LNLS, Campinas, Brazil). The radiation wavelength was set to 0.148 nm and a MarCCD detector (bi-dimensional position-sensitive detector) was used to record the scattering patterns. The sample-to-detector distance was set to  $\sim 1000\text{ mm}$  allowing us to explore a scattering vector interval from 0.11 to 3.3  $\text{nm}^{-1}$ , where  $q$  is the magnitude of the scattering  $q$ -vector defined by  $q = (4\pi/\lambda)\sin\theta$  ( $2\theta$  being the scattering angle). In this way, the maximum Bragg distance accessible from our experimental set-up was *circa* 60 nm. Samples were set between two mica



windows and a 1 mm spacer, handled in a liquid sample-holder placed perpendicular to the incoming beam. The obtained curves (data collection of 5 minutes) were normalized by taking into account the X-ray beam intensity decrease during the experiment. The scattering curve of the phosphate buffer solution was subtracted from the sample's SAXS curves, considering each sample's attenuation. All measurements were taken at room temperature of 22 °C.

For the SAXS data analysis we assume here that the scattering objects can be represented by hollow cylinders as nanotubes. It is noteworthy that such a cylindrical symmetry for the peptide aggregates is further confirmed by molecular dynamics simulations. Therefore, the SAXS intensity  $I(q)$  from a solution of long cylinders such that  $L \gg 10D_{cs}$ , where  $L$  and  $D_{cs}$  are the cylinder length and cross-section diameter, respectively, can be written as<sup>27,28</sup>

$$I(q) = k n_p P(q) S(q), \quad (1)$$

where  $n_p$  corresponds to the particle number density and  $k$  is a normalization factor related to the instrumental effects.  $P(q)$  and  $S(q)$  in eqn (1) are the scattering particle form factor and structure factor, respectively. In our case, the  $P(q)$  function parameters for long hollow cylinders are the inner and outer cylinder radii, namely  $R_{in}$  and  $R_{out}$ , respectively, which define the layer thickness ( $= R_{out} - R_{in}$ ) comprising the peptides and hydration water.<sup>27,28</sup> Furthermore, this model is implemented in GENFIT software.<sup>29</sup> For a two-dimensional hexagonal lattice with cell parameter  $a$ , the  $S(q)$  function is correlated with the Bragg diffraction peak positions centered at<sup>30</sup>

$$q_{hk} = (4\pi/a(3)^{1/2})(h^2 + hk + k^2)^{1/2} \quad (2)$$

with  $h$  and  $k$  being the Miller indices. Therefore, in this case, the scattering intensity exhibits Bragg peaks, whose positions in the reciprocal space relative to the position of the first peak are 1,  $\sqrt{3}$ , 2,  $\sqrt{7}$  and so on, corresponding to  $d_{10}$ ,  $d_{11}$ ,  $d_{20}$ ,  $d_{21}$  interplanar distances, respectively ( $d_{hk} = 2\pi/q_{hk}$ ).

Interestingly, Freiburger and Glatter<sup>30</sup> described the scattering intensity of the hexagonal-like arrangement exhibiting pronounced Bragg peaks dependent on both the height and width of the Bragg peaks. This was named as the multi-peak model, first derived by Forster *et al.*<sup>31</sup> and implemented in the GIFT (Generalized Inverse Fourier Transform) software.<sup>30</sup> According to such methodology, it is possible to derive the number of coherent scattering cylinders and the degree of disorder caused, for instance, by thermal fluctuations.<sup>30,31</sup>

Here we made use of such methodology in such a way that the fitting parameters to the SAXS experimental data are: the cylinder cross-section dimension, the cylinder-cylinder mean distance corresponding to the lattice constant  $a$ , and the lattice vibrations related to the thermal vibrations. It is noteworthy that thermal vibrations can be understood as distortions on the lattice position of the rigid cylinders.<sup>30,31</sup> Such distortions are understood as oscillations around an equilibrium position, giving rise to a relative mean square displacement,  $\sigma_a^r$ . Thus, the final fitting parameter is the total

mean square displacement,  $\sigma_a$ , which can be written as  $\sigma_a = a\sigma_a^r$ .<sup>31</sup> Finally, as in the proposed model the cylinder is much longer than its cross-section dimension, the latter is considered to be monodisperse.<sup>30</sup> A more detailed description of this model can be found elsewhere.<sup>30,31</sup>

## 2.4 Molecular dynamics simulation

The self-organizing properties of the GHRP-6 peptide were evaluated using coarse-grained molecular dynamics (CG-MD) simulations using the MARTINI forcefield<sup>32</sup> and its extension to proteins,<sup>33</sup> as implemented in the Gromacs 4 package.<sup>34</sup> The systems were simulated using a 20 fs timestep, under NPT conditions using Berendsen thermostat and barostat.

Simulations were conducted starting from a random distribution of the peptides on a cubic water box with phosphate ions to neutralize the system and to mimic the experimental conditions. Thus, following such a procedure, it is possible to get more details on the peptide behavior during the self-assembly process. Additional simulations were started from the peptide aggregates reorganized into pentagonal arrangements.

## 3. Results

### 3.1 Cryo- and conventional transmission electron microscopy

Cryo-TEM (Fig. 2A–C) and TEM (Fig. 2D) micrographs obtained from samples composed of 20 mg mL<sup>-1</sup> of GHRP-6, in the presence of phosphate buffer at pH 7.4, reveal that bundles of long linear structures are formed. Furthermore, magnification of a part of such structures is displayed in Fig. 2B, evidencing a lower electron density region along the longitudinal direction with respect to the outer region of the peptide aggregate. Such a finding can be associated with the formation of hollow aggregates. This point will be better explored by means of SAXS measurements and molecular dynamics simulations later in the text.

Fig. 2E and F depict the inner and outer cross-section dimensions of the linear aggregates with the best Gaussian fits (solid lines) to the histograms for the Cryo-TEM and TEM analyses, respectively. Such values as well as the corresponding thicknesses of the aggregates are displayed in Table 1. As one can observe from Fig. 2E and F, the distribution of the cross-section dimensions of the GHRP-6 aggregates is quite monodisperse. According to TEM, the outer and inner dimensions are 14.2(6) and 7.0(7) nm, respectively (Fig. 2E), whereas the thickness amounts to 3.6(3) nm. Regarding Cryo-TEM measurements, the outer and inner cross-section dimensions and the thickness are 11.9(8), 5.8(7) and 3.1(4) nm (Fig. 2F), respectively.

With the aim of better evaluating the main structural features of the peptide aggregate as well as the mechanism that promotes its self-assembly, small-angle X-ray scattering experiments and molecular dynamics simulation were thus carried out, as follows.

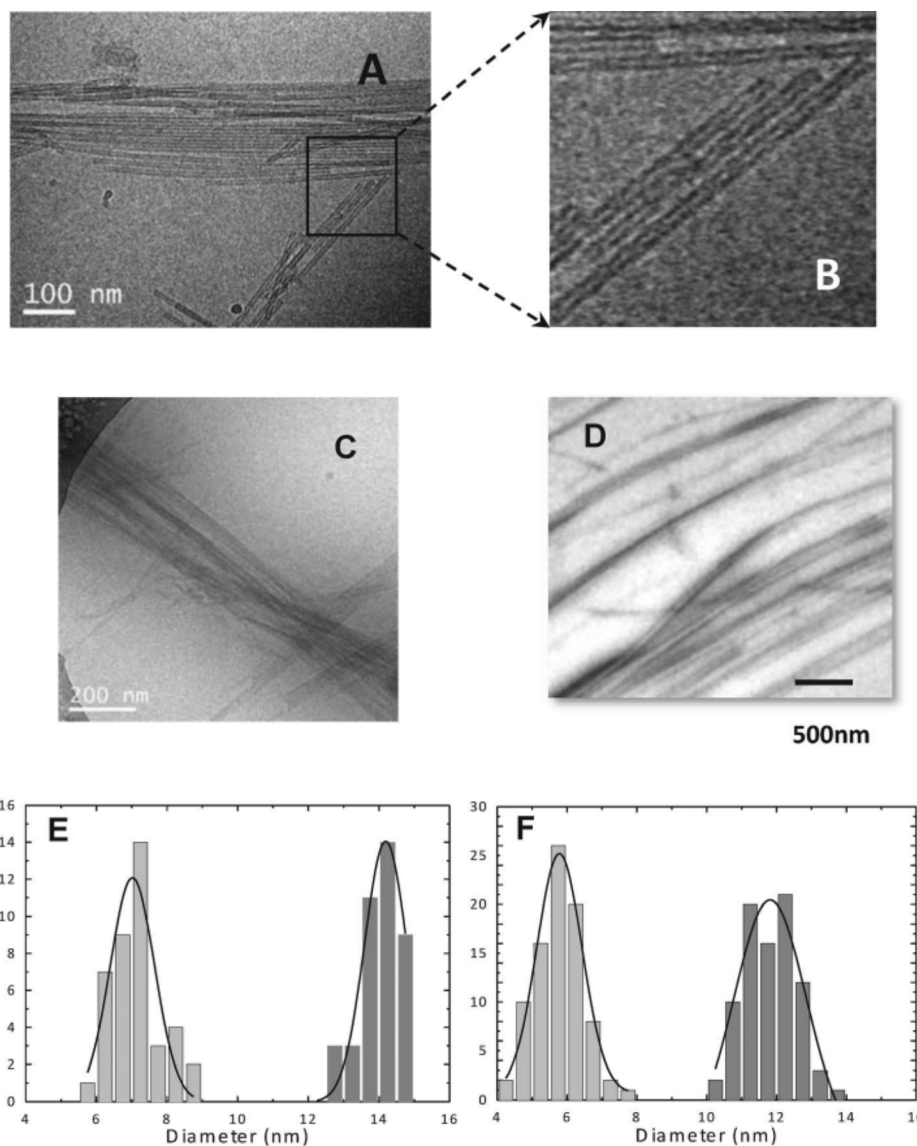


**Fig. 2** Cryo-Transmission Electron Microscopy (A–C) and Transmission Electron Microscopy (D) images of GHRP-6, 20 mg mL<sup>-1</sup> in phosphate buffer solution at pH 7.4. Inner (light grey) and outer (dark grey) cross-section distribution histogram for the linear aggregates obtained from the analysis of TEM (E) and Cryo-TEM (F), respectively. The solid lines in E and F are the best Gaussian fits for each distribution. The adjustment parameters can be appreciated in Table 1.

**Table 1** Comparison of external and inner cross-sections of the GHRP-6 self-assembled aggregate, as well as its thickness, obtained using Cryo-TEM, TEM, SAXS and MDS (molecular dynamics simulation) techniques with the associated standard deviation<sup>a</sup>

	Cryo-TEM	TEM	SAXS	MDS
External cross-section (nm)	11.9 (8)	14.2 (6)	13.4 (5)	15.0
Inner cross-section (nm)	5.8 (7)	7.0 (7)	7.4 (2)	9.0
Thickness (nm)	3.1 (4)	3.6 (3)	3.0 (2)	3.0

<sup>a</sup> The values in parentheses represent the standard deviation.

### 3.2 SAXS

SAXS measurements were performed at peptide concentrations ranging from 20 to 70 mg mL<sup>-1</sup> at pH 7.4 in 20 mM phosphate

buffer. Samples with smaller concentrations did not yield a detectable SAXS signal after one day of sample preparation. Fig. 3A shows the scattering curve from 20 mg mL<sup>-1</sup> of GHRP-6 along with the best model fitting supposing that the peptides self-assemble into long hollow cylinder-like aggregates, which represent the hollow linear structures observed by electron microscopy (Fig. 2). Of note, a homogeneous cylinder model was also employed as an attempt to fit the experimental data. Nevertheless, it failed to reproduce the broad peak centered at  $q \sim 0.75 \text{ nm}^{-1}$  in the scattering curve (data not shown). Such a broad peak is typical of the scattering of either hollow or core-shell structures.<sup>35,36</sup>

According to the modeling, the cylinder inner radius and the peptide-containing shell thickness resulted to be, respectively, 3.7(2) nm and 3.0(2) nm (inset in Fig. 3A), which indicated an



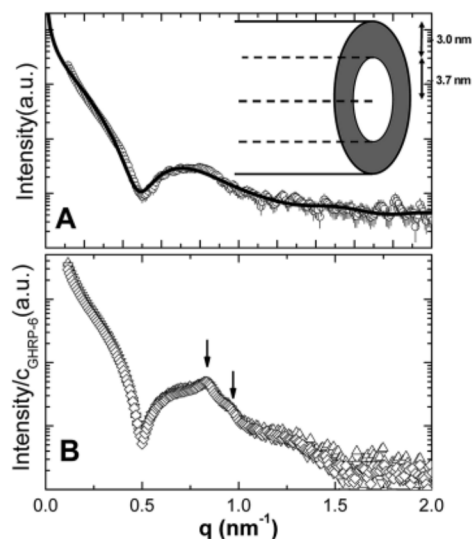


Fig. 3 (A) Scattering curve from GHRP-6 at 20 mg mL<sup>-1</sup> in phosphate buffer solution (open circles), pH 7.4, along with the best fitting considering a long hollow cylinder-like model (solid line). A schematic representation of the hollow cylinder cross-section can be appreciated in the inset, within the main dimensions of the cylinder. (B) Concentration-normalized SAXS curves of GHRP-6 at 30 ( $\Delta$ ), 50 ( $\nabla$ ) and 70 mg mL<sup>-1</sup> ( $\diamond$ ) at pH 7.4 in phosphate buffer. The arrows indicate the position of the visible Bragg peaks. See text for further details.

outer cylinder cross-section of 6.7(2) nm, in good agreement with electron microscopy results (Table 1). In this way, the cylinder wall thickness of 3.0(2) nm determined by SAXS could accommodate two GHRP-6 molecules partially stacked or interpenetrated, considering that the extended length of the GHRP-6 molecule is  $\sim 2$  nm, calculated from the  $C_{\alpha}$  of His1 to the  $C_{\alpha}$  of Lys6 as measured with VMD software, see Fig. 1. Thus, it is possible that GHRP-6 behaves as a surfactant-like peptide, *i.e.*, it self-assembles in bilayers on the cylinder wall, resulting in a nanotube-like aggregate with a total external diameter of  $\sim 13.4(5)$  nm. We will return to this point when discussing molecular dynamics simulation results later on in the paper.

As the GHRP-6 concentration increases from 30 mg mL<sup>-1</sup> to 70 mg mL<sup>-1</sup> (Fig. 3B), it is possible to notice the appearance of Bragg peaks at  $q \sim 0.83$  nm<sup>-1</sup> and  $0.96$  nm<sup>-1</sup> in the normalized SAXS curves (arrows in Fig. 3B). Interestingly, the SAXS curves' profiles are not affected by increasing the peptide amount. One should bear in mind that the peak position defines the average distance among the interacting structures, which in the present study is the hollow-cylinder center-to-center position. Thus, as the Bragg peaks' position remains unaltered when the peptide concentration increases, the mean distance between the center-to-center hollow-cylinders also remains the same regardless of the GHRP-6 concentration. Therefore, an increase in the peptide concentration leads to an increase in the nanotube long dimension, without affecting its cross-section.

Regarding the position of the Bragg peaks, if we consider the first diffraction peak centered at  $q \sim 0.83$  nm<sup>-1</sup>, the mean distance between the interacting nanotubes would be smaller than their cross-section with no physical meaning. On the other hand, with the assumption that these two peaks (arrows in

Fig. 3B) correspond, indeed, to a second and third order of a local hexagonal liquid-crystal packing, the first diffraction peak should lie at  $q_{10} = 0.48$  nm<sup>-1</sup>, which is very close to the minimum of the hollow-cylinder form factor at  $q \sim 0.5$  nm<sup>-1</sup> (Fig. 4A). Thereby, the experimental diffraction peaks observed at  $q \sim 0.83$  nm<sup>-1</sup> and  $0.96$  nm<sup>-1</sup> are related to the (11) and (20) plane reflections of the hexagonal 2D-packing (Fig. 4A). The dashed-vertical lines in Fig. 4 evidence the position of the first three peaks from a hexagonal arrangement. In order to better infer some physical parameters of the hexagonal packing, we use the methodology developed by Freiburger and Glatter<sup>30</sup> to analyse the SAXS curves by retrieving the  $S(q)$  and  $P(q)$  functions, concomitantly.

By doing so, Fig. 4A shows the best fitting (solid line) to the SAXS data from 70 mg mL<sup>-1</sup> GHRP-6 dispersed in aqueous solution along with the  $P(q)$  function (dashed line), as an example, whereas Fig. 4B displays the resulting  $S(q)$  function, with the following parameters: the lattice parameter,  $a = 15.2$  nm, the domain size  $D \sim 63$  nm, and the mean lattice deviation  $\sigma_a \sim 1.8$  nm, whereas the cylinder cross-section was 13.4(5) nm, in accordance with the SAXS result. As one can note, the main peak of the  $S(q)$  function is indeed coincident with the minimum of the  $P(q)$  function. The corresponding unit cell parameter  $a$  of 15.2 nm related to the center-to-center distance between two adjacent hollow-cylinders (see the scheme in the inset of Fig. 4A) indicates a water layer of

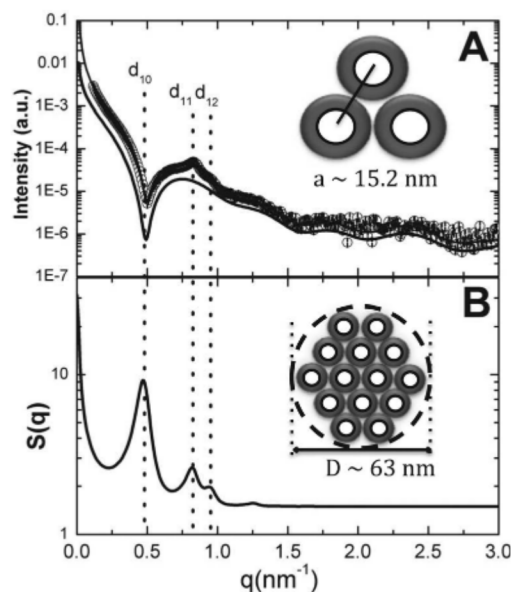


Fig. 4 (A) SAXS curves of GHRP-6 at 70 mg mL<sup>-1</sup> (open spheres) along with the best fitting obtained using the hexagonal model described by Freiburger and Glatter,<sup>30</sup> fitting eqn (1). In the inset one can see the average center-to-center distance of each hollow-cylinder. The dotted line (A) is the hollow cylinder form factor,  $P(q)$ , whereas the solid line in panel B is the cylinder-cylinder interference function,  $S(q)$ . In the inset of panel B one can see a schematic representation for the average interacting hollow-cylinders within a domain, obtained using the approach developed by Freiburger and Glatter.<sup>30</sup> The dashed lines show the correspondence between the peaks of the  $S(q)$  in B and the experimental scattering curve.

*circa* 1.4(5) nm separating two adjacent nanotubes (*i.e.* the wall-to-wall distance), taking into account that the total cylinder cross-section dimension is around  $\sim 13.4(5)$  nm. Such a finding reveals a quite narrow water interface between the hollow cylinders. Besides, the domain size ( $\sim 63$  nm) is on the same order of magnitude as the lattice parameter  $a$  ( $\sim 15.2$  nm), suggesting that there are a small number of interacting cylinders, which is also justified by the broad Bragg peaks (see the scheme in the inset of Fig. 4B). In fact, using a rough approximation, from the domain size,  $D$ , combined with the unit cell dimension,  $a$ , it is possible to suggest that an average number of  $\sim 13$  cylinders in solution are short-range correlated giving rise to the hexagonal-like pattern observed. It is noteworthy that the structural features of the peptides remain unaltered, despite the changes in the peptide concentration.

Furthermore, the intensities of the high-order reflections are damped due to deviations from the ideal lattice positions.<sup>31</sup> Such deviations can be mathematically modeled using the Debye–Waller factor, as described elsewhere.<sup>31</sup> In the present study, such deviations are mainly due to thermal fluctuations of the cylinder's mean positions being equal to  $\sim 1.8$  nm, in accordance with the mean wall-to-wall distance among the adjacent cylinders. Taking together, the SAXS results indicate that the hollow-cylinders are interacting with an average distance slightly larger than the hollow-cylinder cross-section comprising a quite small bundle of cylinders.

The agreement between SAXS and transmission electron microscopy results is quite remarkable, as shown in Table 1. From TEM values obtained over dried samples and Cryo-TEM data collected over quickly frozen samples without solvent removal, we can infer that the GHRP-6 aggregates retain their structure following transfer from aqueous solution to the solid support.

### 3.3 Molecular dynamics simulation

Modeling self-assembly of molecules at the atomic level using computational techniques has remained a challenge, due to the time scales needed to simulate the process, in the order of micro to milli seconds, and the large number of particles involved. In this regard, the development of coarse-grained force fields using either implicit or explicit water for the representation of the system made it possible to model the self-assembly of lipids,<sup>37</sup> peptides,<sup>38,39</sup> and proteins.<sup>40</sup> Among all the coarse-grained models developed for proteins, nicely reviewed by Tozzini<sup>40</sup>, we chose the MARTINI force-field<sup>32,33</sup> which has been proven to be useful in reproducing the assembly properties of several biomolecular systems.<sup>33</sup> This coarse-grained force field offers the possibility to perform unconstrained MD simulations of the assembly process providing an unbiased sampling. Briefly, the force field maps four heavy atoms into one interaction particle and has been parametrized focusing on reproducing the partition free energy between apolar and polar phases. The simplifications introduced in the representation of the system provide a four-fold speed-up factor when compared with all-atom simulations. In this work we use this effective time that has been estimated based on the diffusion coefficient of coarse-grained water compared to real water.

Fig. 5A–D depict the time evolution of a peptide solution starting from random positions (Fig. 5A), showing that immediately after 2  $\mu$ s (Fig. 5D) a phase separation between GHRP-6 and water takes place. Furthermore, its cross-section has a circular shape, resembling the structure assumed in SAXS data analysis. Nevertheless, it is not possible, with such information, to describe the peptide–peptide interaction that leads to such an arrangement. This point will be better discussed later on in the text.

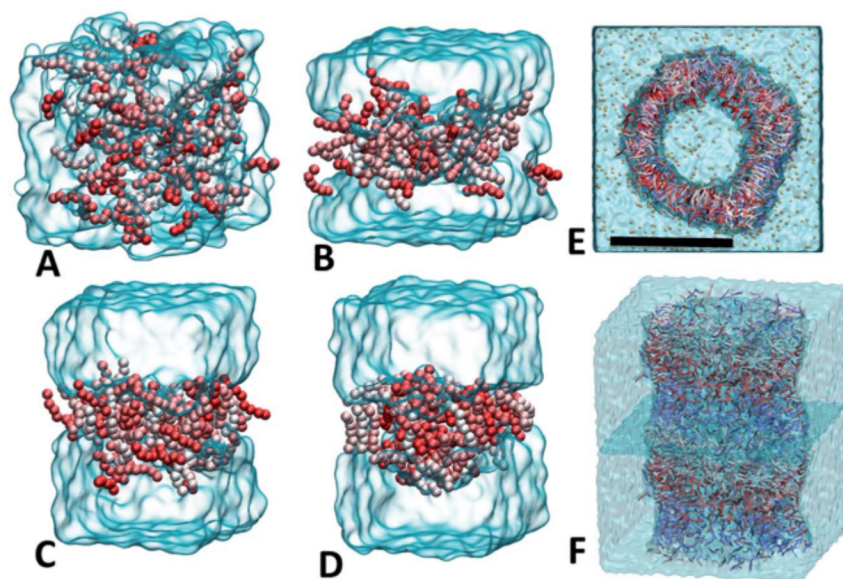
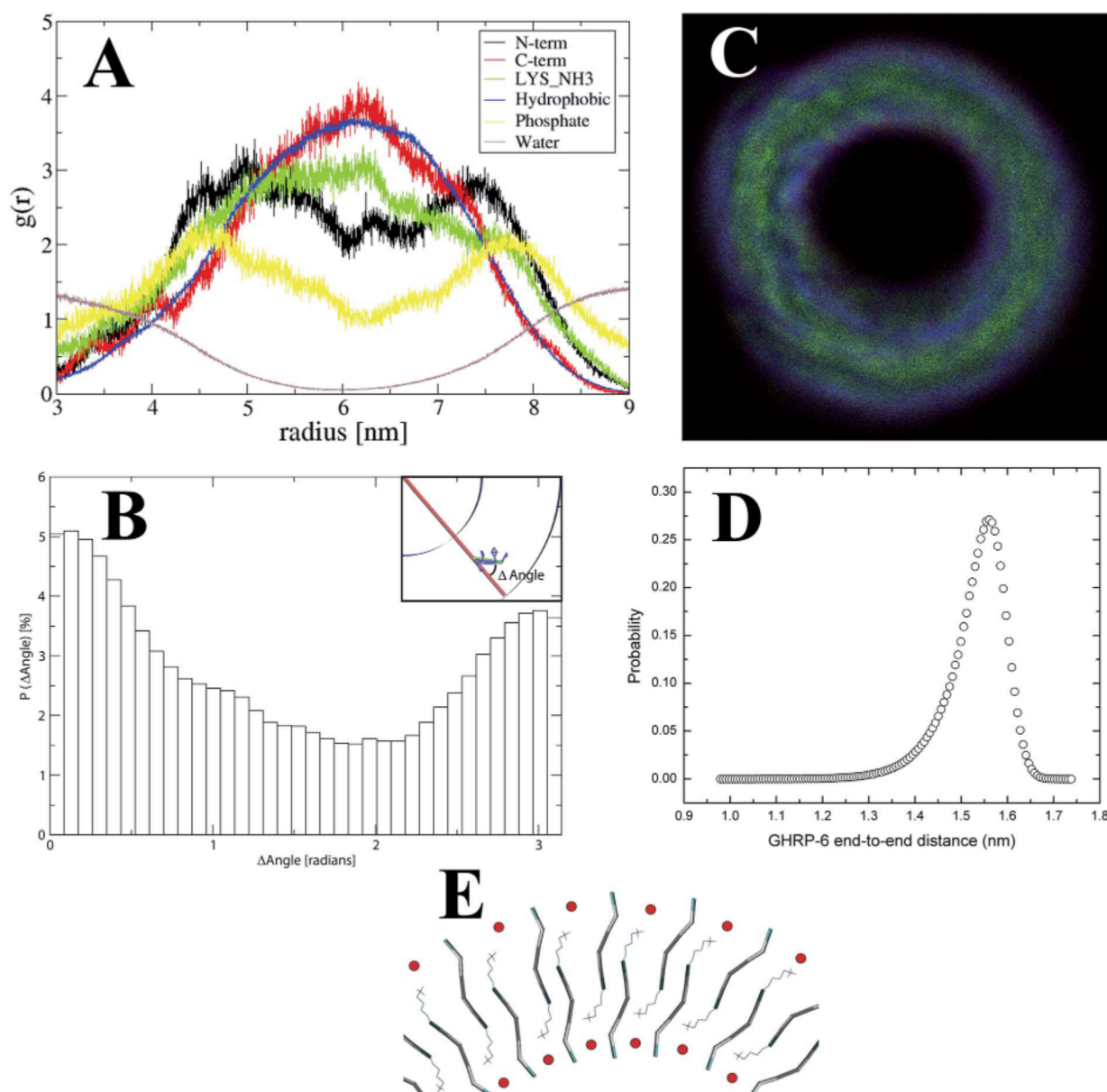


Fig. 5 Snapshots of the spontaneous aggregation of the GHRP-6 peptide in a simulation box at (A) 0 ns, (B) 150 ns, (C) 300 ns and (D) 500 ns. (E) Backbone representation of the peptide in a cylindrical aggregate after 20  $\mu$ s of simulation. (F) Cross-section of the cylinder after 20  $\mu$ s of simulation. The bar in figure E has a scale of 10 nm.



To further evaluate the structural properties of the peptide within a cylindrical arrangement, the peptide layer was replicated using a cylindrical symmetry along the  $z$ -axis and simulated for additional 100  $\mu\text{s}$  (Fig. 5E and F). This procedure was carried out to guarantee that such an arrangement is stable at longer times, *i.e.* 100  $\mu\text{s}$ . Interestingly, after a period of  $\sim 20$   $\mu\text{s}$  the structure is stable, and within the remaining 80  $\mu\text{s}$  no significant changes were found. In contrast to the smaller system described above, an ordering of the peptide within the hollow-cylinder becomes evident, as shown in Fig. 5F.

The radial distribution function,  $g(r)$ , is a powerful tool to study the mean distance between different residues or even atoms, in order to get further information on the peptide organization within the cylinder wall. On this ground, Fig. 6A shows the  $g(r)$  function from the cylinder's center of mass for some relevant components of the system. The inner and outer radii of the hollow cylinder, taken from the peaks in the distribution of the outermost layer of the peptide, are 4.5 nm and 7.5 nm respectively. The similitude in the cylinder's wall thickness (3.0 nm), among all experimental and theoretical approaches, is quite impressive, see Table 1. It thus suggests



**Fig. 6** (A) Radial distribution function  $g(r)$  from the cylinder's center of mass of selected peptide segments, see figure legend for further details. (B) Probability density distribution of the angle formed between the peptide's longest axis and the radial vector. (C) Density map across the plane perpendicular to the cylinder's long axis depicting the mean position of His1 (blue), Lys6 (green) and PHO (red). (D) Probability density function calculated for the GHRP-6 backbone end-to-end distance  $P(r)$ . The mean distance is 1.53(6) nm averaged over time for all the peptides within the nanotube. (E) Schematic representation of the arrangement of the peptides into the cylinder wall. Phosphate ions are depicted in red, the N-terminus is depicted in cyan, while the Lys side-chain is shown in stick representation.



that even though there might be a slight deviation in the packing of the peptides, this simplified theoretical model is able to reproduce the probable distribution of the peptide within the nanotube wall. The external and internal walls of the cylinder, corresponding to the peptide–water interface, are preferentially populated with the amino terminus of the peptide, while the amide-capped carboxy terminus remains buried within the core of the cylinder. Although the core is hydrophobic, as denoted by the absence of water between 5 and 7 nm in  $g(r)$  (Fig. 6A), the positive charges of the amino group in the side chain of Lys stretch out to the peptide–water interface where it is neutralized by phosphate ions. The arrangement of the Lys side chain is reminiscent of the snorkeling behavior described in transmembrane helices embedded in lipidic membranes.<sup>41</sup> An ordering of the peptides into the nanotube wall is also noticed when analyzing the orientation of the vector defined along the peptide chain as compared with that along the radial direction, from the cylinder's center of mass up to the peptide's center of mass (Fig. 6B). Fig. 6B shows the probability distribution function of the angle formed between these two vectors for all peptides during the last 20  $\mu$ s of simulation. There are two peaks in the distribution, 0 and  $\pi$  radians, corresponding to the peptides pointing inside/outside the cylinder's center of mass, respectively. Such an analysis indicates that the peptide is pointing parallel to the radial direction (Fig. 6B).

Fig. 6C shows the electron density map along the cylinder's cross-section, showing the N-terminus (blue channel) at the water–peptide interface, while the C-terminus (green channel) is located in the core. Thus, taking together, these results indicate that GHRP-6 behaves like an amphiphilic molecule in solution, forming a partially interdigitated wall, where the N-terminus is located at the peptide–water interface (His residue) and the C-terminus at the core (Lys residue), while the positive charges arising from  $\text{NH}_3^+$  from the inner Lys groups are neutralized by phosphate ions. Furthermore, Fig. 6D shows the probability density function,  $P(r)$  calculated for the peptides within the hollow-cylinder wall. The average value is 1.53(6) nm, and one can notice an asymmetrical distribution for  $P(r)$  (Fig. 6D).

It is noteworthy that the hexagonal arrangement for the cylinders at higher concentrations, evidenced by SAXS, could be explained based on the charge distribution within the cylinder wall, *i.e.*, the positive His residues are neutralized by the phosphate ions at the surface, favoring the cylinder–cylinder interaction, giving rise to the hexagonal arrangement evidenced by SAXS.

## 4. Discussion

There is a large amount of research dealing with the self-assembly properties of peptides in solution due to the emergent biotechnological applications.<sup>1,17,42,43</sup> Interestingly, in a pioneer study, Santoso *et al.*<sup>44</sup> studied the self-assembly properties of surfactant-like peptides with different glycine (from 4 up to 10 residues) tails (corresponding to the hydrophobic portion) and aspartic acid as the constituent of the negatively charged polar

head group.<sup>44</sup> The authors evidenced that all studied molecules formed either nanotubes or nanovesicles in solution. Moreover, the polydispersity of these structures was dependent on the length of the glycine tail,<sup>44</sup> and in general their cross-section was found to be  $\sim 50$  nm. In our case, GHRP-6 forms thinner hollow-cylinders which are monodisperse in size.

Center *et al.*,<sup>45</sup> on the other hand, studied the influence of trifluoroacetate (TFA) salt on the heptapeptide (Ala)<sub>6</sub>Lys, which has six alanine residues forming the peptide “hydrophobic tail” and one lysine residue representing the polar head group. The authors evidenced that the peptides self-assemble as hollow cylinders with an inner radius of *circa* 26.0(1.3) nm and a wall thickness  $< 1.0$  nm.<sup>45</sup> The self-assembly is highly cooperative and the peptides are distributed in a two-dimensional crystal, which is cylindrically bent,<sup>45</sup> with the peptide aligned along the cylinder surface and perpendicular to the radial direction. Thus, the observed small wall thickness is due to the relative position of the peptide in the hollow cylinder wall. One should bear in mind that although (Ala)<sub>6</sub>Lys is an amphiphilic molecule, it does not exhibit a surfactant-like behavior in the cylinder wall. For instance, Middleton *et al.*<sup>7</sup> obtained similar results, when they studied the architecture of peptide nanotubes formed by the same heptapeptide (Ala)<sub>6</sub>Lys using solid state nuclear magnetic resonance, SSNMR, Fourier transform infrared spectroscopy, FTIR, and transmission electron microscopy, TEM. The authors evidenced that the (Ala)<sub>6</sub>Lys nanotubes had a cross-section of  $\sim 23$  nm, in accordance with the value observed by Center *et al.*<sup>45</sup> They also proposed that the peptides self-assemble into nanotubes constructed from monolayers, the inner water region and the cylinder wall thickness being equal to 20 and  $\sim 3$  nm, respectively.<sup>7</sup> In this case, the peptide is also aligned along the cylinder surface, *i.e.*, perpendicular to the cylinder radial direction. Moreover, the authors were also able to infer that the peptides are organized in a  $\beta$ -strand conformation with a 4.7 Å strand spacing (antiparallel  $\beta$ -sheets),<sup>7</sup> compatible with the small cylinder wall.

In contrast, in the present study we clearly show that the mechanism of self-assembly of short peptides is not general but depends on the peptide amino-acid sequence. In our case, we were able to show that GHRP-6 behaves as an amphiphilic molecule such that the hexapeptide self-assembles parallel to the cylinder radial direction in the non-aqueous environment, forming a thinner nanotube with respect to others reported in the literature.

## 5. Conclusions

In this study we combine bioinformatics with experimental data to investigate how the growth hormone releasing hexapeptide, GHRP-6, associates in aqueous solution. We experimentally show that at 20 mg mL<sup>-1</sup> GHRP-6 self-assembles into very long hollow-cylinders that are at least a few hundreds of nm long after 1 day of sample preparation. According to the SAXS technique, for larger peptide concentrations ( $> 30$  mg mL<sup>-1</sup>), the shape of the long aggregates remains the same, but bundles of nanotubes are disposed in a hexagonal arrangement in solution, with a very well defined center-to-center distance of

~15 nm. Of note, neither twisted nor helical aggregates were observed by electron microscopy as often proposed for amyloid-like peptides.<sup>26</sup> Furthermore, according to molecular dynamics simulations a peptide orientation along the cylinder-shell was proposed to be perpendicular to the cylinder surface, similar to an interdigitated bilayer as depicted in Fig. 6E. Thus, GHRP-6 can be considered as an amphiphilic hexapeptide with two charged groups at physiological pH (corresponding to the NH<sub>3</sub> groups at the N-terminus and the Lys side chain) located in the ends of the polypeptide chain and one hydrophobic core composed of four residues (D-Trp-Ala-Trp-D-Phe) (Fig. 1). Such a composition is probably responsible for the interdigitation, since both charges were partially exposed to water (Fig. 6E).

## Acknowledgements

Authors thank CNPq, and FAPESP for financial support. The authors are also indebted to Prof. Paolo Mariani and Francesco Spinozzi, both from Università Politecnica delle Marche, Ancona, Italy, who provided us the GENFIT software. RI and LRSB are recipients of the CNPq research fellowship. IC, NV and JV acknowledge financial support from DGI (Spain) project Be-Well (CTQ2013-40480-R) and Instituto de Salud Carlos III, through "Acciones CIBER". The Networking Research Center on Bioengineering, Biomaterials and Nanomedicine (CIBER-BBN) is an initiative funded by the VI National R&D&I Plan 2008–2011, Iniciativa Ingenio 2010, Consolider Program, CIBER Actions and financed by the Instituto de Salud Carlos III with assistance from the European Regional Development Fund. Technical support from the SAXS beam line of the Laboratório Nacional de Luz Síncrotron, LNLS (Brazil) and the Microscopy Service of UAB (Cryo-TEM images (Spain)) are also acknowledged. Fig. 1 was made with VMD software support. VMD is developed with NIH support by the Theoretical and Computational Biophysics group at the Beckman Institute, University of Illinois at Urbana-Champaign.

## References

- 1 A. Dehsorkhi, V. Castelletto, I. W. Hamley, J. Seitsonen and J. Ruokolainen, *Langmuir*, 2013, **29**, 14246–14253.
- 2 S. Zhang, *Nat. Biotechnol.*, 2003, **21**, 1171–1178.
- 3 T. A. Doll, S. Raman, R. Dey and P. Burkhard, *J. R. Soc., Interface*, 2013, **10**, 20120740.
- 4 M. R. Ghadiri, J. R. Granja, R. A. Milligan, D. E. McRee and N. Khazanovich, *Nature*, 1993, **366**, 324–327.
- 5 X. Zhao, F. Pan, H. Xu, M. Yaseen, H. Shan, C. A. Hauser, S. Zhang and J. R. Lu, *Chem. Soc. Rev.*, 2010, **39**, 3480–3498.
- 6 S. Scanlon and A. Aggeli, *Nano Today*, 2008, **3**, 22–30.
- 7 D. A. Middleton, J. Madine, V. Castelletto and I. W. Hamley, *Angew. Chem.*, 2013, **52**, 10537–10540.
- 8 A. Mishra, Y. H. Loo, R. S. Deng, Y. J. Chuah, H. T. Hee, J. Y. Ying and C. A. E. Hauser, *Nano Today*, 2011, **6**, 438.
- 9 Y. L. Yang, U. Khoe, X. M. Wang, A. Horii, H. Yokoi and S. G. Zhang, *Nano Today*, 2009, **4**, 193–210.
- 10 C. A. E. Hauser and S. G. Zhang, *Chem. Soc. Rev.*, 2010, **39**, 2780–2790.
- 11 Y. Y. Lin, Y. Qiao, P. F. Tang, Z. B. Li and J. B. Huang, *Soft Matter*, 2011, **7**, 2762–2769.
- 12 J. F. Miravet, B. Escuder, M. D. Segarra-Maset, M. Tena-Solsona, I. W. Hamley, A. Dehsorkhi and V. Castelletto, *Soft Matter*, 2013, **9**, 3558–3564.
- 13 A. Mahler, M. Reches, M. Rechter, S. Cohen and E. Gazit, *Adv. Mater.*, 2006, **18**, 1365–1370.
- 14 G. Fichman and E. Gazit, *Acta Biomater.*, 2014, **10**, 1671–1682.
- 15 A. C. Coleman, J. M. Beierle, M. C. Stuart, B. Macia, G. Caroli, J. T. Mika, D. J. van Dijken, J. Chen, W. R. Browne and B. L. Feringa, *Nat. Nanotechnol.*, 2011, **6**, 547–552.
- 16 A. Trent, R. Marullo, B. Lin, M. Black and M. Tirrell, *Soft Matter*, 2011, **7**, 9572–9582.
- 17 V. Castelletto, I. W. Hamley, C. Whitehouse, P. J. Matts, R. Osborne and E. S. Baker, *Langmuir*, 2013, **29**, 9149–9155.
- 18 I. W. Hamley, *Soft Matter*, 2011, **7**, 4122–4138.
- 19 K. Cheng, W. W. S. Chan, A. Barreto, E. M. Convey and R. G. Smith, *Endocrinology*, 1989, **124**, 2791–2798.
- 20 Y. T. Shen, J. J. Lynch, R. J. Hargreaves and R. J. Gould, *J. Pharmacol. Exp. Ther.*, 2003, **306**, 815–820.
- 21 J. Berlanga, D. Cibrian, L. Guevara, H. Dominguez, J. S. Alba, A. Seralena, G. Guillen, E. Lopez-Mola, A. Rodriguez, B. Perez, D. Garcia and N. S. Vispo, *Clin. Sci.*, 2007, **112**, 241–250.
- 22 T. Niidome, N. Morimoto, S. Iijima, A. Akaike, T. Kihara and H. Sugimoto, *Eur. J. Pharmacol.*, 2006, **548**, 1–8.
- 23 D. G. del Barco, H. Perez-Saad, V. Rodriguez, J. Marin, V. Falcon, J. Martin, D. Cibrian and J. Berlanga, *Neurotoxic. Res.*, 2011, **19**, 195–209.
- 24 J. P. Crow, N. Y. Calingasan, J. Y. Chen, J. L. Hill and M. F. Beal, *Ann. Neurol.*, 2005, **58**, 258–265.
- 25 E. Beghi, T. Mennini, C. Bendotti, P. Bigini, G. Logroscino, A. Chio, O. Hardiman, D. Mitchell, R. Swingler, B. J. Traynor and A. Al-Chalabi, *Curr. Med. Chem.*, 2007, **14**, 3185–3200.
- 26 E. T. Pashuck and S. I. Stupp, *J. Am. Chem. Soc.*, 2010, **132**, 8819–8821.
- 27 A. Guinier and G. Fournet, *Small Angle Scattering of X-rays*, Wiley, New York, 1955.
- 28 O. Glatter and O. Kratky, *Small Angle X-ray Scattering*, Academic Press, London, New York, 1982.
- 29 F. Spinozzi, C. Ferrero, M. G. Ortore, A. De Maria Antolinos and P. Mariani, *J. Appl. Crystallogr.*, 2014, **47**, 1132–1139.
- 30 N. Freiburger and O. Glatter, *J. Phys. Chem. B*, 2006, **110**, 14719–14727.
- 31 S. Forster, A. Timmann, M. Konrad, C. Schellbach, A. Meyer, S. S. Funari, P. Mulvaney and R. Knott, *J. Phys. Chem. B*, 2005, **109**, 1347–1360.
- 32 S. J. Marrink, H. J. Risselada, S. Yefimov, D. P. Tieleman and A. H. de Vries, *J. Phys. Chem. B*, 2007, **111**, 7812–7824.
- 33 L. Monticelli, S. K. Kandasamy, X. Periole, R. G. Larson, D. P. Tieleman and S. J. Marrink, *J. Chem. Theory Comput.*, 2008, **4**, 819–834.
- 34 B. Hess, C. Kutzner, D. van der Spoel and E. Lindahl, *J. Chem. Theory Comput.*, 2008, **4**, 435–447.

- 35 C. O. Rangel-Yagui, H. W. Hsu, L. R. Barbosa, W. Caetano, A. Pessoa Jr, L. C. Tavares and R. Itri, *Pharm. Dev. Technol.*, 2007, **12**, 183–192.
- 36 S. C. Gandini, E. L. Gelamo, R. Itri and M. Tabak, *Biophys. J.*, 2003, **85**, 1259–1268.
- 37 Y. Wang, J. K. Sigurdsson, E. Brandt and P. J. Atzberger, *Phys. Rev. E: Stat., Nonlinear, Soft Matter Phys.*, 2013, **88**, 023301.
- 38 R. B. Pandey, Z. Kuang and B. L. Farmer, *PLoS One*, 2013, **8**, e70847.
- 39 R. S. Hissam, B. L. Farmer and R. B. Pandey, *Phys. Chem. Chem. Phys.*, 2011, **13**, 21262–21272.
- 40 V. Tozzini, *Curr. Opin. Struct. Biol.*, 2005, **15**, 144–150.
- 41 E. Strandberg and J. A. Killian, *FEBS Lett.*, 2003, **544**, 69–73.
- 42 V. Castelletto, I. W. Hamley, M. D. Segarra-Maset, C. B. Gumbau, J. F. Miravet, B. Escuder, J. Seitsonen and J. Ruokolainen, *Biomacromolecules*, 2014, **15**, 591–598.
- 43 A. Dehsorkhi, V. Castelletto and I. W. Hamley, *J. Pept. Sci.*, 2014, **20**, 453–467.
- 44 S. Santoso, W. Hwang, H. Hartman and S. G. Zhang, *Nano Lett.*, 2002, **2**, 687–691.
- 45 C. C. Cenker, S. Bucak and U. Olsson, *Soft Matter*, 2011, **7**, 4868–4875.